Clays and Clay Minerals, Vol. 52, No. 4, 451–461, 2004.

BIOMIMETIC CO-ASSEMBLY OF GIBBSITE AND MESOPHASES: A NOVEL SYNTHESIS ROUTE BY DEVITRIFICATION OF GEL DERIVED FROM HYDROTHERMAL ALUMINOSILICATE/CTAB SOLUTION

YAUH-YARNG FAHN[1], POUYAN SHEN[2,*] AND AN-CHUNG SU[2]

[1] Department of Chemical Engineering, Tung-Fang Institute of Technology, Eastern College of Technology and Commerce, Hu-Nei, Kaohsiung 829, Taiwan

[2] Institute of Materials Science and Engineering, National Sun Yat-sen University, Kaohsiung, Taiwan

Abstract—The effect of an amphiphilic surfactant on the co-assembly of gibbsite and low-dimensional-order, liquid-crystalline mesophases using a hydrothermal-gelation-devitrification route was examined. Crystal growth by this method occurred either in three dimensions or was limited to only two dimensions. Gibbsite and mesophases were synthesized using a cationic surfactant, cetyltrimethyl ammonium bromide (CTAB), as template and a commercial mineral sample as inorganic precursor. The commercial mineral sample contained pyrophyllite, α-quartz, and minor kaolinite. The syntheses were made at pH 10 under hydrothermal conditions followed by equilibration at room temperature. The hydrothermally soluble portion settled at room temperature to form a translucent hydrous gel. This translucent gel turned white after drying on a glass substrate because of the following events based on chemical analysis, X-ray diffraction, and optical/electron microscopy: (1) gibbsite preferentially nucleated at the gel/air and gel/glass interfaces to form spherulites of tabular gibbsite crystals with entrapped droplets; (2) a ~26 Å basal-spacing, aluminate-encased, lamellar mesophase formed by 2D growth near the edge of the drying gel; and (3) residual solution in entrapped droplets within the gibbsite phase later devitrified abruptly into an optically isotropic material (an aluminosilicate gel possibly with minor mesophases) with a dendritic morphology. Formation of gibbsite and the lamellar mesophase was initially interface controlled, but later became 2D diffusion-controlled as CTAB concentrations and micelle lengths were increased with crystallization time. A relatively high surfactant/water ratio of the drying gel might account for predominant crystallization of an aluminate-encased lamellar mesophase rather than the hexagonal mesophase known as the Mobil Composition Material MCM-41.

Key Words—Biomimetic Co-assembly, Gel Devitrification, Gibbsite, Aluminosilicate and CTAB Solution, Mesophase, Polarized Optical Microscopy, Transmission Electron Microscopy.

INTRODUCTION

The motivation for this research was to study the effects of the amphiphilic surfactant CTAB and growth dimensionality (*i.e*. crystal growth in three dimensions or constrained to only two dimensions) on the competitive assembly of gibbsite and aluminate/aluminosilicate-encased mesophases using a hydrothermal-gelation-devitrification route with a commercial aluminosilicate mineral sample as inorganic precursor. The mineral sample was naturally occurring and beneficially low-cost for the fabrication of gibbsite and/or mesoporous materials.

Mesophases are materials that have low-dimensional, liquid-crystalline order states. Surfactant templates and inorganic precursors have been used widely in the past decade to synthesize inorganic-encased mesophases using a hydrothermal route. The regular array of uniform mesopores revealed after template removal have potential applications as mesoporous molecular sieves (Beck *et al*., 1992) due to their very high surface area and adsorption capacity. The pioneering work for this synthesis method, by Kresge *et al*. (1992), used a cationic surfactant (hexadecyltrimethylammonium, also called cetyltrimethylammonium) and an inorganic precursor to form particulates with an hexagonal array of uniform mesopores with silicate walls that is known as the Mobil Composition Material MCM-41. The MCM-41 also formed tubules-within-a-tubule using a similar route but with an extra acidification step after treatment under alkaline conditions (Lin and Mou, 1996). The inorganic (typically silicate or aluminosilicate)-encased and surfactant-leached particles of MCM-41 with 2D crystal symmetry (plane group *p6mm*) have adjustable mesopore size via surfactant selection and synthesis condition. In contrast, conventional microporous materials, such as the zeolites, are restricted to a specific fine intracrystalline pore size which is not more than 14 Å for the mineral cacoxenite (Moore and Shen, 1983). Formation of this mesoporous molecular sieve in hydrothermal solution involves a liquid crystal (more or less silicatropic) mechanism, as indicated by *in situ* ^{29}Si NMR (Chen *et al*., 1993), morphological (Cheng *et al*., 1995) and *in situ* X-ray diffraction (XRD) (Rathousky *et al*., 1999) observations. It was found

* E-mail address of corresponding author:
pshen@mail.nsysu.edu.tw
DOI: 10.1346/CCMN.2004.0520406

that the heating time necessary for the synthesis of stable MCM-41 decreases with increasing synthesis temperature up to 110ºC in autoclaves and liquid crystalline materials without a silicatropic signature do not survive heating to 95ºC (Chen *et al*., 1993). The hexagonal silicatropic liquid crystalline phase (SLC), formed in the presence of charged silicate oligomers present during the production of MCM-41 (Chen *et al*., 1993; Firouzi *et al.*, 1995), was generally accepted as derived from a lamellar mesophase (Monnier *et al.*, 1993) or disordered intermediate (Brown *et al.*, 1997). On the other hand, the hexagonal SLC in the form of colloidal columnar particles was found to accrete by Brownian motion and imperfect attachment over {10} surfaces and base to produce dislocations, twist boundaries, and faceted pores, typically ~50 nm in size (Shen *et al.*, 2001).

We used the hydrothermal synthesis route to prepare well-ordered MCM-41 material (Lin and Mou, 1996), but used clay as the inorganic precursor. We chose a commercial mineral sample (pyrophyllite, α-quartz, with minor kaolinite) as an inorganic precursor in order to study the assembly of aluminate/aluminosilicate-encased mesophases as well as gibbsite. Gibbsite ($Al(OH)_3$) is commonly encountered in the hydrothermal or sol-gel synthesis of alumina (Yamaguchi *et al*., 1966). Gibbsite also occurs in bauxite formed from rocks in weathering environments (Valeton, 1972). The Bayer process begins with bauxite ore to produce aluminum trihydrate (i.e. hydrargillite or gibbsite) after treatment with caustic soda solutions and then calcined to form alumina (Flock, 1978; Veesler and Boistelle, 1994). Gibbsite formation was examined using Monte Carlo simulations with a 2D nucleation model (Sweegers *et al*., 2002). It is of interest to discover whether the aluminate lamellar phase or MCM-41 can be synthesized using a surfactant/inorganic moiety and the Al^{3+} leached from pyrophyllite and kaolinite at high pH to form $Al(OH)_4^-$ and/or AlO_2^-, rather than by leaching at low pH (Yada *et al*., 1996, 1997). The competitive crystallization of gibbsite and mesophases under the influence of CTAB and growth dimensionality during gel dehydroxylation on a glass substrate was studied via in-situ optical polarized microscopy. We focused on the co-assembly and microstructural development of gibbsite/mesophase from gel rather than precursor aluminosilicate/CTAB/H_2O solution.

EXPERIMENTAL METHODS

Synthesis

A commercial mineral sample (Showa Company, 300 mesh, 72.10% SiO_2, 19.57% Al_2O_3, and <2.48% CaO; 3.70 SiO_2/Al_2O_3 weight ratio) was used as the inorganic precursor in the surfactant/inorganic moiety synthesis route. This material contains pyrophyllite, α-quartz and minor kaolinite, based on XRD (Figure 1). Approximately 10 g of Showa material and 7.2 g of CTAB were added to 100 mL of water and stirred for 3 h in a polypropylene beaker. The solution was then allowed to stand at room temperature for 24 h to sediment into a two-layer mixture. The top aqueous layer was enriched in the surfactant, colloids and other soluble materials and the bottom layer contained residual Showa material with silt-size grains. The top solution layer was immediately sealed in a polypropylene bottle for further chemical measurements. Quantitative analysis using inductively coupled plasma optical emission spectroscopy (ICP-OES, Perkin-Elmer, Optima 2000 DV) indicated that the translucent upper layer contained 3.4 ppm Al and 8.3 ppm Si. (The measured 3.4 ppm Al and 8.3 ppm Si concentrations were probably from suspended colloidal particles of the Showa sample, *i.e.* predominantly pyrophyllite, because the Si:Al ratio of 8.3/3.4 = 2.44 is similar to that of pyrophyllite (2.35)).

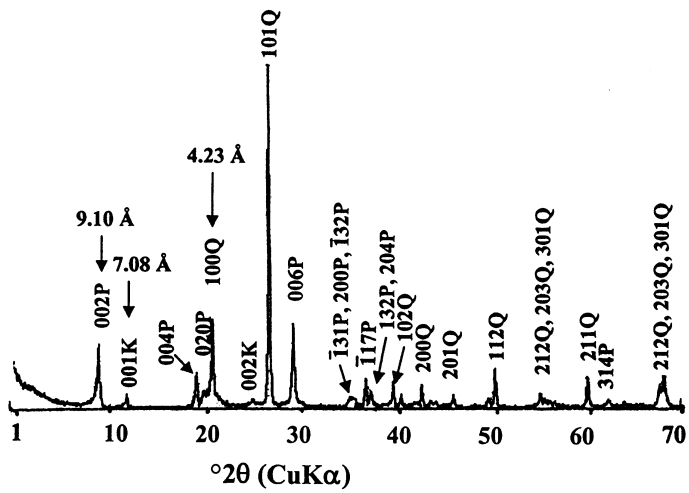

Figure 1. XRD profiles of Showa material with α-quartz (Q), pyrophyllite (P) and minor kaolinite (K). The *d* spacings of the representative peaks for each phase are indicated (Å).

https://doi.org/10.1346/CCMN.2004.0520406 Published online by Cambridge University Press

The translucent upper layer was then separated by filtration through a Buchner funnel, 1 N NaOH was added until the pH was 12.4, then back titrated with 1 M H_2SO_4 to pH 10.0. The resulting solution was then heated to 100ºC for 72 h in an autoclave in a stainless steel container to form a colloidal solution and later a hydrous gel. The ICP-OES analysis of the colloidal solution that was initially formed revealed 20 ppm Al and 46 ppm Si and indicates that hydrothermal treatment increased the concentrations by nearly six times the initial values. The acidification of a CTAB/inorganic salt solution followed by hydrothermal treatment in an autoclave has previously been used to form an hexagonal, well-ordered, aluminosilicate mesophase in the form of tubules-within-a-tubule by Lin and Mou (1996). We simply followed this acidification and hydrothermal route to study the effect of using a different inorganic precursor. Gibbsite and a lamellar mesophase rather than a hexagonal mesophase were predominantly created from the gel. Another experiment starting at pH 10 gave basically the same results.

Structural characterization

X-ray diffraction (CuKα radiation at 40 kV and 30 mA, in the 10−100º2θ range) was used to study the crystal structures of the synthesized gel powders more or less crystallized when overlaid on a glass slide at room temperature. Powder XRD was also conducted in the 1−10º2θ range for detailed characterization of inorganic encased mesophases, *i.e.* lamellar and/or hexagonal phases with relatively large *d* spacings. Transmission electron microscopy (TEM, using a JEOL 3010 instrument operated at 300 kV over template-cleaned powders settled on a C-coated collodion film supported by a Cu grid), scanning electron microscopy (SEM, using a JSM-6400 instrument operated at 20 kV) and point-count energy-dispersive X-ray (EDX) analysis were used to characterize the microstructures and composition of surfactant-leached particulates. Gelation, dehydroxylation and devitrification of the colloidal solution droplets overlaid on a glass plate were monitored at room temperature via optical microscopy under plane-polarized light. In an additional 'blank' experiment, the aqueous CTAB solution (0.37 M in concentration) devoid of the inorganic ingredients was allowed to react in a stainless steel container sealed with Teflon at 100ºC for 3 days; the resultant gel dried on a glass plate was then examined for its crystallization behavior.

RESULTS

Based on visual inspection of three independent experimental runs, the hydrous inorganic/CTAB gel produced via this hydrothermal method was homogeneous and transparent but became a translucent gel within minutes of ageing at room temperature. Subsequent devitrification was manifested by the continuous emergence of nuclei at the gel-air interface followed by the spherulitic growth of white, tabular gibbsite crystals which grew up to 1 cm in size overnight at the expense of the drying gel. The structure, microstructures and composition of the gibbsite as well as mesophases in the devitrified gel were characterized by XRD of the sample powder and microscopic observations of the coatings on a glass slide. A combination of evidence from XRD, EDX and optical microscopy observations under plane-polarized light (*i.e.* interference color, extinction angle and birefringence (Fahn, 2000)) support the identification of gibbsite and mesophases as delineated in the following.

X-RAY DIFFRACTION OF DEVITRIFIED POWDER GEL

Results from XRD of the dehydroxylated and devitrified gel derived from the top layer of the aluminosilicate/CTAB/H_2O solution subjected to hydrothermal treatment indicated the co-existence of a predominant lamellar mesophase, a moderate amount of gibbsite (Figure 2), and negligible hexagonal mesophase as revealed in the low 1−10º2θ range (inset in Figure 2). The gibbsite has the same basal layer spacing as the monoclinic crystal (space group $P2_1/n$) precipitated from hot sodium aluminate solution (JCPDS file 12-460), in accord with the SEM-EDX result of negligible Si and CTAB contents. On the other hand, the lamellar mesophase has a slightly smaller basal layer spacing than that (26 Å) of pure CTAB (JCPDS file 30-1746), indicating that it is inorganic-encased. The minor hexagonal mesophase, presumably also inorganic encased, has a tubular interspacing of 47 Å based on $2/3^{1/2}$ times the *d* spacing of the 10 peak, which would correspond to the 100 and $10\bar{1}$ reflection in the *hkl* (Kresge *et al.*, 1992) and (*hki*) (Shen *et al.*, 2001) indexing scheme, respectively. Note that 2D Miller indices (*hk*) were used here to index the diffraction peaks of the hexagonal mesophase with plane group *p6mm* (Shen *et al.*, 2001). Generally, both selected-area electron diffraction (SAED) and XRD patterns show only a few low-order members of the *hk*0 subset of hexagonal reflections in the *hkl* scheme (Kresge *et al.*, 1992). Upon template leaching with ethanol, the gibbsite remained, whereas the lamellar/hexagonal mesophases were hardly detected by XRD (Fahn, 2000).

Optical microscopic observations of gel devitrification

In general, gibbsite crystals and the lamellar mesophase grow rather quickly from the colloidal solution if allowed to flow and dry on a glass plate. When viewed edge-on under cross polarization, the gibbsite flake exhibits clino-extinction (maximum extinction angle = 42º), length fast and higher interference color than the top view, in accord with its refraction indicatrix and the monoclinic structure of the crystal (Winchell and

https://doi.org/10.1346/CCMN.2004.0520406 Published online by Cambridge University Press

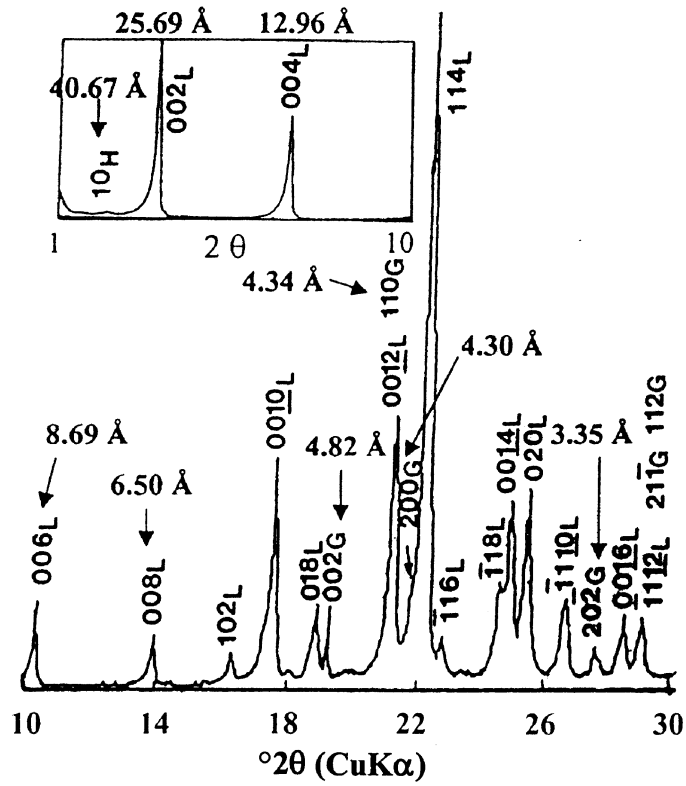

Figure 2. XRD profiles of the gel powder hydrothermally synthesized from the aluminosilicate/CTAB solution, followed by dehydroxylation and devitrification at room temperature, showing the coexistence of gibbsite (G), the aluminate-encased lamellar phase (L), and a rather small amount of hexagonal mesophase (H). The inset is an expanded view of the low-angle range 1−10°2θ to show lamellar and hexagonal mesophases. The *d* spacing values are labeled next to the predominant peaks for each phase.

Winchell, 1961; Deer *et al.*, 1992). Conoscopic observation indicated a 2V angle of almost zero and a positive optic sign. The lamellar mesophase when viewed edge-on also exhibits length-fast and clino-extinction with a maximum extinction angle of ~42°. Unambiguous distinction of gibbsite from the lamellar mesophase, however, may be achieved by noting differences in the growth habit (*i.e.* spherulitic *vs.* dendritic as well as twinning *vs.* non-twinning) and its dependence on CTAB concentration.

When the CTAB/water ratio and viscosity were relatively low, as in humid weather conditions or in the early stage of devitrification in a thick colloidal solution coating, formation of gibbsite flakes was preferred. In this case, it is common to find gibbsite crystals widened and thickened in a rather anisotropic manner, with fluid inclusions of various sizes entrapped within the crystals. Similar to residual solution open to air (addressed later), the fluid relics as inclusions in gibbsite crystals allow further development of mesophases. Polysynthetic twinning on (100) or (110) planes was observed in the top-view (*i.e.* down the *c* axis) for some gibbsite flakes, showing alternating extinction across the twin plane (Fahn, 2000). The growth rate of the tabular gibbsite in this stage was found to be between 0.1 and 1 mm/h, two to three orders higher than that via spiral growth (Lee and Parkinson, 1999) and that from hydrothermal alumina caustic solutions (Veesler and Boistelle, 1994). In general, spherulitic gibbsite was found to develop from the tabular gibbsite nuclei until impingement (Figure 3). The impinged spherulites thus formed on the glass plate were typically <500 μm in size, much smaller than those formed in a container with less drying. In contrast, growth dimensionality decreased as the surfactant/water ratio increased at the edge of the spreading colloidal solution and a brushlike, dendritic lamellar mesophase was formed (Figure 4). Solution evaporation and quick growth of the lamellar mesophase (i.e. up to 1 mm within seconds) frequently caused rapid retreat of the solution edge.

Both the gibbsite and lamellar mesophase particles were much smaller, but more numerous (*i.e.* more nuclei with a slow growth rate) after the solution became viscous after ageing (with or without air conditioning) at room temperature for up to 3 h. Under such circumstances, the crystals were found to nucleate predominantly at the viscous flow front. In a separate drying experiment of a rather viscous fluid on a glass slide, we monitored the sequential devitrification time in step increments of ~20 s. As shown in Figure 5, two euhedral gibbsite crystals with anisotropic relief (Figure 5a) acted as nuclei for the brownish and optically isotropic phase.

https://doi.org/10.1346/CCMN.2004.0520406 Published online by Cambridge University Press

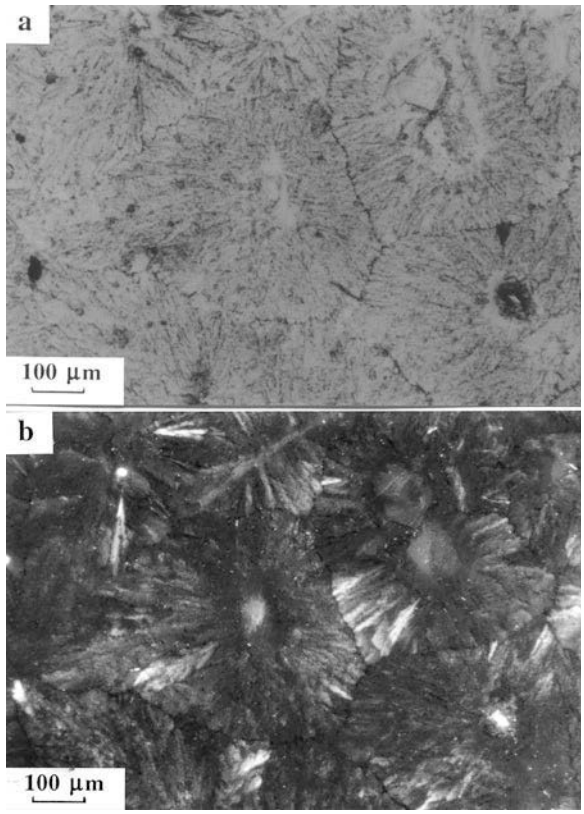

Figure 3. Optical micrograph of impinged gibbsite spherulites developed from the tabular gibbsite nuclei. (a) open polarizer, (b) crossed polarizers.

The gibbsite crystals became elongated hexagons due to slight growth-rate differences between the (100) and (110) faces caused by defects or impurities as in surfactant-free hydrothermal solutions (Lee and Parkinson, 1999). The gibbsite crystals then thickened in a rather stepwise manner via a spiral growth mechanism while the supercooled fluid became brownish. Subsequently, another gibbsite crystal, with a dendritic shape due to a lower viscosity in the surrounding fluid, developed in the upper part (Figure 5b). Finally, in the amorphous solution residue, explosive and fractal-like growth of isotropic material (dark brown in color under open polarizer) was observed (Figure 5c). This may be attributed to either diffusion-limited aggregation or radial distribution fingers. The brownish material is optically isotropic, as indicated by complete extinction under crossed polarizers (Figure 6). The SEM-EDX analysis indicates that this optically isotropic material is aluminosilicate, possibly a gel with minor inorganic-encased mesophases. It is noteworthy that an incubation time was required for this type of fractal growth. When it formed, the amorphous solution residue was instantaneously covered with this brownish material, leaving impinged gibbsite spherulites (up to 100 µm in size) unstained.

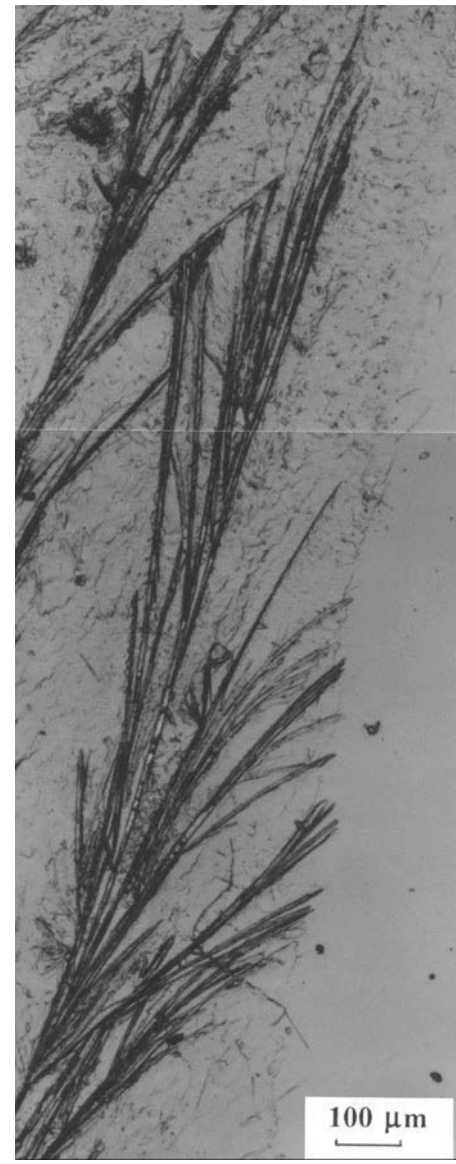

Figure 4. Optical micrograph, under open polarizer, demonstrating the development of dendritic lamellar mesophase upon drying (on a glass slide) of colloidal solution with a relatively high CTAB/H_2O ratio.

In the additional 'blank' experiment, aqueous CTAB solution droplets spread and dried on a glass slide also indicated the dependence of devitrification on drying. It was found that the lamellar mesophase is hexagonal in the early stages (Figure 7a), and the particles are later impinged with one another (Figure 7b). In the final stage, especially near the flow front, the lamellar mesophase became dendritic (Figure 7c), as in the case of aluminate-encased ones. The lamellar mesophase thus prepared contains pores and decomposes at a lower temperature (250ºC) than that of the aluminate-encased phase (274ºC) according to thermogravimetric analysis (at a heating rate of 10ºC/min) of gel powders

https://doi.org/10.1346/CCMN.2004.0520406 Published online by Cambridge University Press

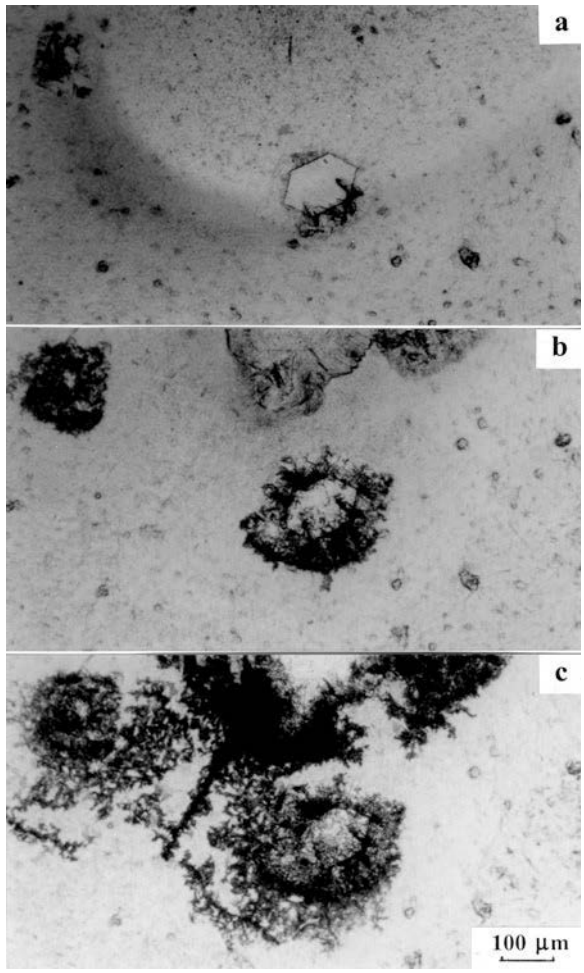

Figure 5. Optical micrographs, under open polarizer, showing sequential devitrification steps to form euhedral gibbsite crystals with brownish rim: (a) 40 s, (b) 100 s, and (c) 120 s.

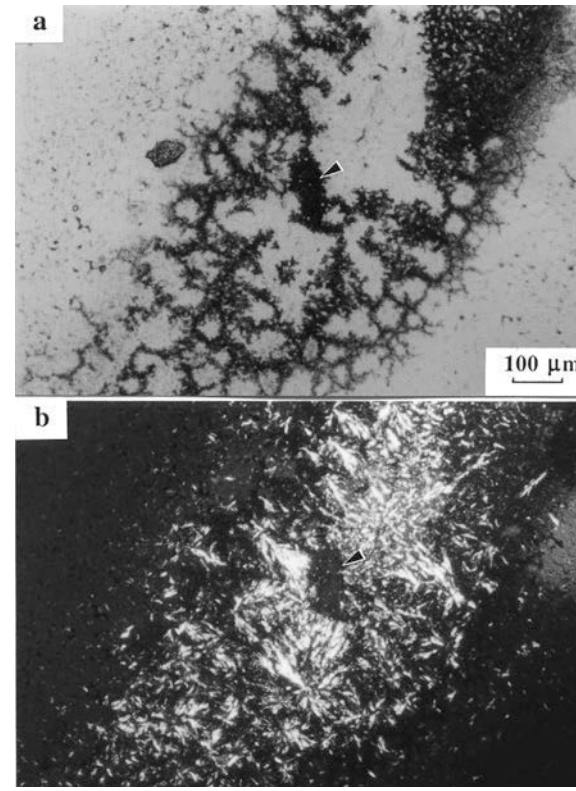

Figure 6. Optical micrographs of optically isotropic brownish hexagonal mesophase (arrow) and spherulitic gibbsite: (a) open polarizer, (b) crossed polarizers.

synthesized in CTAB/H_2O and CTAB/aluminosilicate/H_2O systems, respectively (Fahn, 2000). A higher dehydration temperature for the lamellar mesophase suggests that incorporation of Al stabilizes the CTAB-templated mesophases.

Electron microscopic analysis

The dendritic lamellar mesophase was identified by means of SEM-EDX analysis to be aluminate-encased (Figure 8). A graphite holder was used to avoid counts that otherwise would come from a soda-lime glass slide. The lamellar mesophase, retrieved from the dendrite at the edge of the devitrified gel and with CTAB partially removed, was confirmed via TEM-EDX analysis as aluminate-encased and CTAB mediated. This aluminate-encased lamellar mesophase is generally assembled in various orientations; the edge-on lamellae revealed a clearly regular spacing of 26 Å in the bright field image (BFI) and 2D Fourier transform of the square region (Figure 9a). The aluminate wall was ~16 Å thick based on the dark fringes in the BFI. It should be noted that a minor hexagonal mesophase with characteristic tubules end-on and dislocations can be identified in the lamellar mesophase, as shown in the reconstructed image (Figure 9b) and schematic drawing (Figure 9c) of the square region.

DISCUSSION

Charged species in equilibrium with pyrophyllite/kaolinite and gibbsite at pH = 10

The point of zero charge (PZC) is at pH = 2 for SiO_2 (silica gel) and at pH = 9.1 for Al_2O_3 (corundum). At pH 10, the negatively-charged AlO_2^- derived from pyrophyllite and kaolinite have similar chemical weathering behaviors in terms of abrasive pH, packing index, or energy index (Loughnan, 1969). At pH 10, the species SiO_4^{4-}, $Al(OH)_4^-$, $H_3SiO_4^-$ and their polymeric forms are available to anchor to the cationic head groups of surfactants. The surfactants are induced by van der Waals attractive force to adopt the flattest possible conformation (Theng, 1974) due to the equilibrium reactions between kaolinite, gibbsite, dissolved silica, and water (Garrels and Christ, 1965; May *et al*., 1979; Lindsay and Walthall, 1996) as discussed below. According to the solubility-pH relationship (Lindsay

https://doi.org/10.1346/CCMN.2004.0520406 Published online by Cambridge University Press

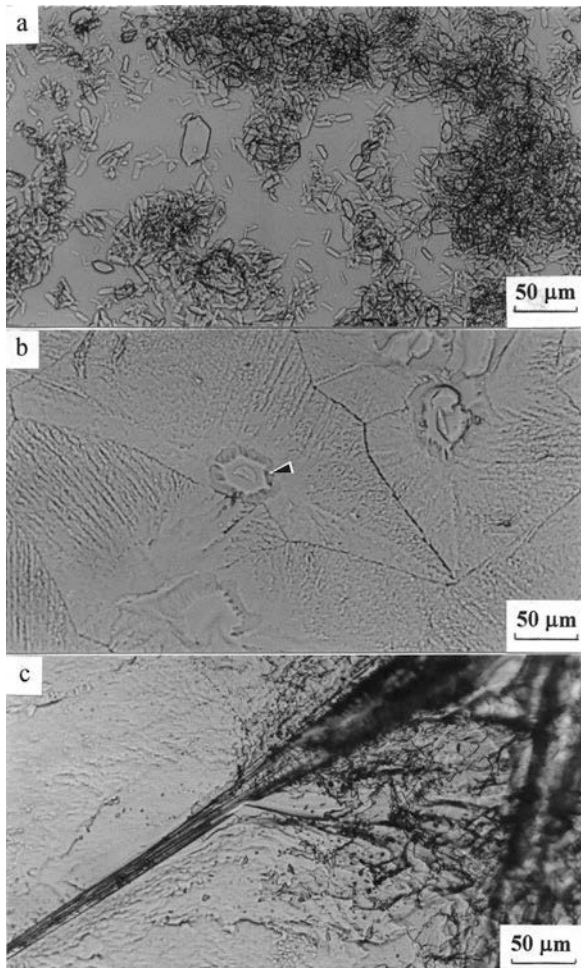

Figure 7. Optical micrograph (open polarizer) of an aqueous CTAB solution droplet spread and dried on a glass slide showing (a) hexagonal lamellar mesophase crystallized in an early devitrification stage, (b) impinged domains of spherulitic lamellar phase with pores (arrow), (c) dendritic lamellar mesophase formed at the flow front.

and Walthall, 1996), nordstrandite, boehmite, gibbsite and diaspore have very similar solubilities. However, gibbsite was found to be the predominant synthesis product according to the present XRD and microscopic characterization. It is an open question whether CTA^+ caused predominant formation of gibbsite at ambient temperature and pressure. In any case, the formation of gibbsite is in accord with its wide occurrence in soils (Lindsay and Walthall, 1996) and its solubility behavior (Garrels and Christ, 1965; May *et al.*, 1979).

The gibbsite-kaolinite stability fields expressed in terms of pH and activities of the dissociation products Al^{3+}, AlO_2^- and H_4SiO_4 at 25ºC and 1 atm indicated a planar boundary between gibbsite and kaolinite representing a fixed activity of H_4SiO_4. At H_4SiO_4 activities greater than this value, kaolinite can be expected to dissolve congruently, and thus to leave no gibbsite residue. The ion activities are equal at pH = 5.1. This may account for the absence of gibbsite in the upper translucent solution, in addition to the effects of CTAB reaction, colloidal particle sedimentation, and temperature in the present hydrothermal aluminosilicate/CTAB solution. In any case, pyrophyllite/kaolinite in the Showa powders should dissolve to yield aluminate ion under alkaline hydrothermal conditions for subsequent formation of aluminate-encased mesophases upon cooling and further dwelling at room temperature.

For weakly acidic solutions with pH > 2 (*i.e.* the PZC of silica), silica particles bear a net negative surface charge and tend to dissolve in water to form simple monomeric complexes such as $Si(OH)_{4\ (aq)}$ and other oligomers or even larger polymers (Iler, 1979). The dissolution of silica involves

$$SiO_2 + 2\ H_2O \rightarrow Si(OH)_{4\ (aq)}$$

with log K = −2.7 for amorphous silica (Iler, 1979). In alkaline solutions, colloidal silica particles are also negatively charged (Iler, 1986). Therefore, we conclude from the above discussion that aluminosilicate dissolution at pH = 10 should yield the negatively charged aluminate and silicate species.

CTAB/H_2O/aluminosilicate sol-gel

Silica at pH 7−10.5 begins to dissolve as silicate and silica particles are negatively charged and repel one another (Iler, 1979). Therefore, particles grow continuously without aggregation. On the other hand, gelation of silica may occur if electrolyte salts are added to shield the repulsion, temperature is decreased to suppress the particle growth, or pH is lowered to decrease the negative surface charge.

Analogously in this study, the upper solution separated from the colloidal aluminosilicate solution became a sol and then a gel upon cooling to room temperature. As mentioned above, the negatively-charged aluminate and silicate species that are present at pH = 10 cannot significantly reduce the negative surface charge of the aluminosilicate sol. Presumably it was the Na^+ and the polar head of the cationic surfactant CTAB that effectively reduced the surface charge of the aluminosilicate sol and encouraged coagulation when the sol was cooled. As for the gel structure, we may neglect the effect of counter ions as a first approximation. It is interesting to note that recent ^{27}Al magic angle spinning nuclear magnetic resonance (MAS NMR), infrared (IR) spectroscopy, and small-angle X-ray scattering (SAXS) measurements of homogeneous aluminosilicate and alumina gels indicate that the former has a fractal network structure, whereas the latter has a non-fractal network built up from aggregates (Sinkó *et al.*, 1999).

Amphiphilic surfactant-like entities (such as CTAB here) may play a crucial role in causing aged colloidal sols to form non-crystalline rather than crystalline products. The effectiveness of the ligands in promoting the formation of non-crystalline products over crystal-

https://doi.org/10.1346/CCMN.2004.0520406 Published online by Cambridge University Press

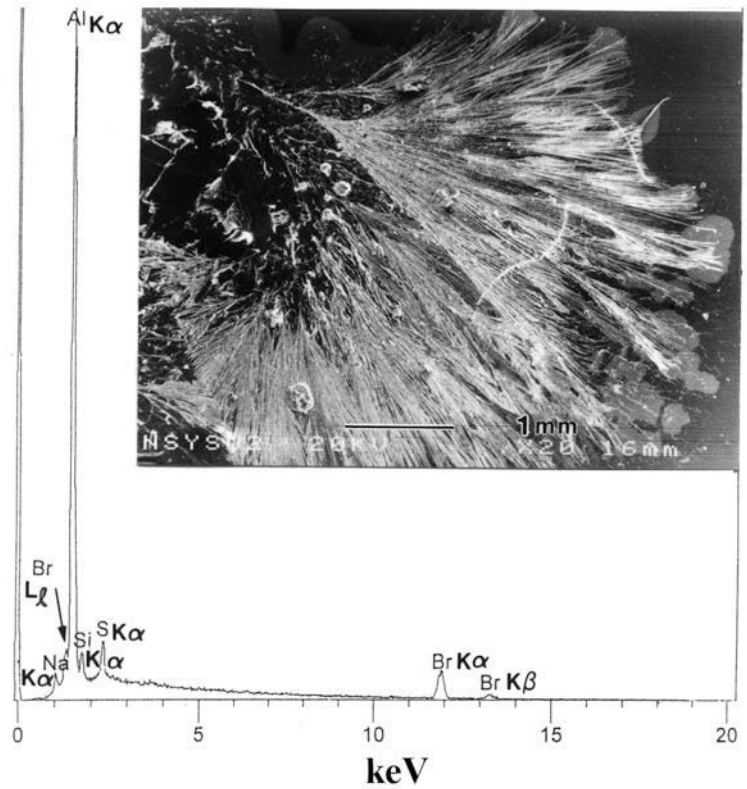

Figure 8. Point-count EDX spectrum and inset SEM image of dendritic and aluminate-encased lamellar mesophase. Note that the Al counts were from the Al sample stub and all other counts were from the colloidal solution residue. The energy unit is keV.

line $Al(OH)_3$ polymorphs (at an initial Al concentration of 2×10^{-3} M at pH = 8.2) follows the order: phthalate $\approx$ succinate < glutamate < aspartate < oxalate < silicate $\approx$ fluoride < phosphate < salicylate ~ malate < tannate < citrate < tartrate (Violante and Huang, 1985). Polydentate and large ligands are generally more inhibitive than those with fewer functional groups or of smaller sizes. Above a critical ligand/Al ratio, crystalline products are inhibited and ligands are coprecipitated with noncrystalline products. Phosphate is also a more effective ligand than silicate for the formation of pseudoboehmite (which is of the same composition as diaspore) over crystalline $Al(OH)_3$ polymorphs such as gibbsite (Violante and Huang, 1985). In the presence of CTAB, polynuclear OH-Al complexes in hydroxyaluminum solutions would probably deviate from the so-called Keggin structure that contains a tetrahedrally coordinated central Al. Keggin structures are typically dominant only in fresh, laboratory-hydrolyzed OH-Al solutions with OH/Al molar ratios $\geqslant 1.8$ (Wang and Hsu, 1994). Subsequent dehydroxylation and devitrification of the gel at room temperature led to an irreversible crystallization path described below.

Crystallization path of gel upon dehydroxylation

At pH 10, the solubility of gibbsite is ~100 ppm whereas the solubility of amorphous silica is ~500 ppm and silica solubility increases further with temperature (Iler, 1979). Although gibbsite and silica solubilities are ionic-strength dependent, it is very likely that AlO_2^-, not SiO_4^{4-}, first became over-saturated. Hence, gibbsite precipitated as the upper, translucent portion of the aluminosilicate/CTAB/H_2O solution formed a gel. The aluminate-incorporated lamellar mesophase could co-assemble via a surfactant-mediated process (see next section) in local regions of relatively high CTAB/H_2O ratios, such as at the water-air interface or in the late dehydroxylation stage. Eventually, concentrations of the negatively charged silicate species became high enough to form a small amount of the hexagonal, aluminosilicate mesophase.

The sol structure or particle size might also play a critical role in initiating the formation of crystalline or amorphous oxide particles (Murrell, 1997). In particular, for the case of aluminas formed from preformed sols there is apparently an upper threshold in size of the sol, which serves to dictate the size of the crystalline alumina particles. Alumina sols below this threshold size lead to polymerization within the gel and formation of much denser alumina structures (Murrell, 1997).

Surfactant-mediated crystallization of gibbsite and lamellar mesophase

Heterogeneous nucleation of gibbsite and lamellar mesophase at the water/air or gel/air interface might

https://doi.org/10.1346/CCMN.2004.0520406 Published online by Cambridge University Press

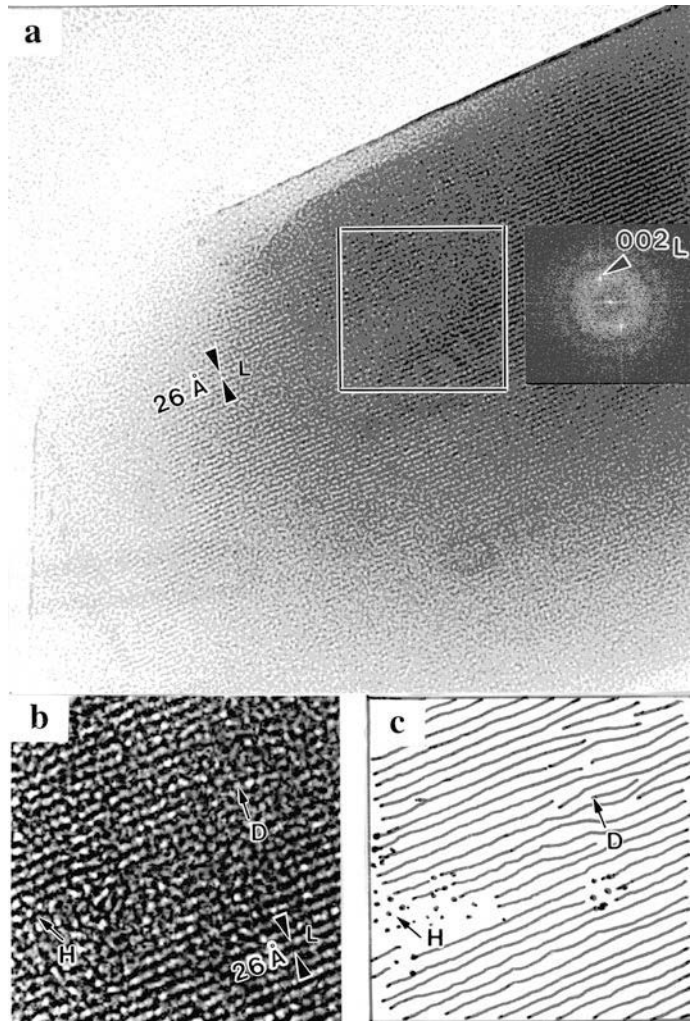

Figure 9. (a) TEM bright-field image and corresponding 2D Fourier transform (inset) from the marked region in a, showing the lamellar 002 spacing of 26 Å, (b) reconstructed image, and (c) schematic drawing from the marked region in a, showing dislocations (denoted as D) and hexagonal mesophase (H) in the matrix of corrugated lamellar mesophase (L).

benefit from a lowering in surface energy and, hence, a lowering in activation energy. Recent X-ray and neutron reflectivity results indicated that the air-water interface mediated silicate multi-layer film is highly ordered in one dimension (Brown *et al.*, 1997, 1998). The process involves an incubation period for the accumulation and ordering of the surfactant and silicate precursor at the interface; this is then followed by the rapid growth of a layered structure showing strong Bragg-like diffraction in the specular reflecting plane (Brown *et al.*, 1997; 1998). In addition, a contribution from elastic strain energy may also become important near the surface of the rigidified gel and cause surface nucleation, reminiscent of surface nucleation of amorphous material below the glass transition temperature (Schmelzer *et al.*, 1993).

In the high-pH range, the negatively-charged surface of the gibbsite or aluminate mesophase wall is expected to cause physical and chemical adsorption (*i.e.* hydrophilic coating) of the long-chain quaternary ammonium cation micelle and is analogous to the silica/CTAB system. The surfactant concentration should be a key factor in rendering both sides of the surfactant micelle-layer hydrophilic and facilitate crystallization. In the case of single-layer adsorption at very low surfactant concentrations, the surface is hydrophobic; only upon formation of double-layered hydrophilic coatings would the surfaces become hydrophilic. In this surfactant-mediated scheme, the growth of gibbsite may involve aggregation of particles into sheets analogous to the case of silica particles (Iler, 1979). In addition, the gibbsite crystal allows no interlayer species as indicated by a constant basal layer interspacing. We note that spiral growth of gibbsite, which is known to operate below a critical super-saturation in surfactant-free hydrothermal solutions (Lee and Parkinson, 1999), is also effective in the presence of a surfactant (Figure 5a) in this study.

https://doi.org/10.1346/CCMN.2004.0520406 Published online by Cambridge University Press

The aluminate-encased hexagonal mesophase has a lamellar spacing in accordance with a double cetyltrimethylammonium$^+$ (CTA^+) layer incorporated with a thin aluminate layer. This indicates conformity of the hydrophobic tail with the aluminate-anchored head group of CTA^+. The formation of tubular micelles (which are the constituent entities of the hexagonal mesophase) is not favored at high CTAB/H_2O ratios. Nevertheless, a minor amount of the hexagonal mesophase was still identified by XRD. Hexagonal mesophase development at high CTAB concentrations may be attributed to formation from a lamellar phase (Monnier *et al*., 1993) or a disordered intermediate (Brown *et al.*, 1997). This is also supported by the present TEM observations (*i.e.* Figure 9).

Growth dimensionality

Colloidal particles can attach to the tabular gibbsite and lamellar mesophase at the edges where the repulsion energy barrier is less than on the faces. This accounts for lateral growth by the ledge mechanism or the so-called 2D nucleation model (Sweegers *et al.*, 2002), based on Monte Carlo simulations, which suggests that the edge (free) energy of the flat faces determines the growth morphology. The importance of each face in morphological development may be arranged in the following order: $(112)/(11\bar{2}) \approx (101)/(10\bar{1}) < (200) < (110) < (002)$ (Sweegers *et al.*, 2002). The present observation of tabular gibbsite crystals is consistent with the formation of 2D nuclei and various lateral surfaces.

Change of crystal growth dimensions from 3D to 2D can also occur when the CTAB/H_2O ratio increases with time or when the overlying solution thins at the edges. In the center of the residual solution droplets, crystals may be nucleated and assembled in 3D to form tabular domains until impingement. In contrast, when growth dimensionality changed from 3 to 2 near the edge, both the gibbsite and lamellar mesophase became dendritic rods (Figure 4). This is analogous to diffusion-limited finger-like growth in a number of systems (Witten and Sander, 1981; Daccord *et al.*, 1986; Fowler, 1990).

CONCLUSIONS

Surfactant-water-mineral interactions are common to both natural (Valeton, 1972) and artificial (Yamaguchi *et al.*, 1966) colloidal solutions. The clay minerals may change shape and phase identity because of the presence of the amphiphilic surfactant. The results of the present study suggest that, in a high-pH environment, the Al^{3+} leached from aluminosilicate is expected to form a peraluminous colloidal solution for subsequent development of gel, mesophases, and aluminate crystals as of major concern to bauxite genesis (Valeton, 1972; Garrels and Christ, 1965). It is an open question whether the presence of a surfactant (whether natural, such as phospholipids (Groves and Boxer, 2002) or artificial, such as CTAB, here) would affect the equilibrium as well as the specific devitrification product formed in natural environments.

In terms of practical applications, we have shown that the surfactant/inorganic moiety synthesis route in an alkaline CTAB/H_2O solution with negatively charged aluminate species could be successfully adopted for the synthesis of aluminate lamellar mesophase and gibbsite, the latter being the key intermediate of Bayer-processed aluminas (Flock, 1978). This route may possibly be extended to dip coating of mesostructured CTAB-aluminate film in a manner similar to the CTAB-silica system (Grosso *et al.*, 2002). The minor hexagonal mesophase is of concern in the fabrication of aluminate MCM-41 materials from natural minerals and additional studies are required to improve the surface area and pore-size distribution. It would be more effective to separate the <2 μm fraction from the Showa material or use a material that largely consists of clay-size particles for a better supply of Al and Si in a future industrial process.

ACKNOWLEDGMENTS

We thank Dr Bill Jaynes and an anonymous referee for constructive comments and extensive editing on the original manuscript. This research is supported by the Center for Nanoscience and Nanotechnology at NSYSU and National Science Council, Taiwan under contract NSC 91-2626-E-272-002.

REFERENCES

Beck, J.S., Vartuli, J.C., Roth, W.J., Leonowicz, M.E., Kresge, C.T., Schmitt, K.D., Chu, C.T-W., Olson, D.H., Sheppard, E.W., McCullen, S.B., Higgins, S.B. and Schlenker, J.L. (1992) A new family of mesoporous molecular sieves prepared with liquid crystal templates. *Journal of the American Chemical Society*, **114**, 10834–10843.

Brown, A.S., Holt, S.A., Dam, T., Trau, M. and White, J.W. (1997) Mesoporous silicate film growth at the air-water interface – direct observation by X-ray reflectivity. *Langmuir*, **13**, 6363–6365.

Brown, A.S., Holt, S.A., Reynolds, P.A., Penfold, J. and White, J.W. (1998) Growth of highly ordered thin silicate films at the air-water interface. *Langmuir*, **14**, 5532–5538.

Chen, C.Y., Burkett, S.L., Li, H.X. and Davis, M.E. (1993) Studies on mesoporous materials II. Synthesis mechanism of MCM-41. *Microporous Materials*, **2**, 27–34.

Cheng, C.F., He, H.Y., Zhou, W.Z., and Klinowski, J. (1995) Crystal morphology supports the liquid crystal formation mechanism for the mesoporous sieve MCM-41. *Chemical Physics Letters*, **244**, 117–120.

Daccord, G., Nittmann, J. and Stanley, H.E. (1986) Radial viscous fingers and diffusion-limited aggregation: Fractal dimension and growth sites. *Physical Review Letters*, **56**, 336–339.

Deer, W.A., Howie, R.A. and Zussman, J. (1992) *An Introduction to the Rock-forming Minerals*. Longman, Essex, England.

Fahn, Y.Y. (2000) Microstructures of mesophases, MCM-41 and gibbsite formed in CTAB/water system with negatively charged silicate and aluminate species. PhD thesis, National Sun Yat-sen University, Taiwan, p. 159.

Firouzi, A., Kumar, D., Bull, L.M., Besier, T., Sieger, P., Huo,

Q., Walker, S.A., Zasadzinski, J.A., Glinka, C., Nicol, J., Margolese, D., Stucky, G.D. and Chmelka, B.F. (1995) Cooperative organization of inorganic-surfactant and biomimetic assemblies. *Science*, **267**, 1138–1143.

Flock, W.M. (1978) Bayer-processed aluminas. Pp. 85–100 in: *Ceramic Processing before Firing* (G.Y. Onoda, Jr. and L.L. Hench, editors). Wiley, New York.

Fowler, A.D. (1990) Self-organized mineral textures of igneous rocks: the fractal approach. *Earth-Science Reviews*, **29**, 47–55.

Garrels, R.M. and Christ C.L. (1965) *Solutions, Minerals, and Equilibria*. Harper and Row, New York.

Grosso, D., Babonneau, F., Albouy, P.A., Amenitsch, H., Balkenende, A.R., Brunet-Bruneau, A. and Rivory, J. (2002) An in situ study of mesostructured CTAB-silica film formation during dip coating using time-resolved SAXS and interferometry measurements. *Chemistry of Materials*, **14**, 931–939.

Groves, J.T. and Boxer, S.G. (2002) Micropattern formation in supported lipid membranes. *Accounts of Chemical Research*, **3**, 149–157.

Iler, R.K. (1979) *The Chemistry of Silica Solubility, Polymerization, Colloid and Surface Properties, and Biochemistry*. Wiley, New York, p. 866.

Iler, R.K. (1986) Inorganic colloids for forming ultrastructures. Pp. 3–20 in: *Science of Ceramic Chemical Processing* (L.L. Hench and D.R. Ulrich, editors). Wiley, New York.

Kresge, C.T., Leonowicz, M.E., Roth, W.J., Vartuli, J.C. and Beck, J.S. (1992) Ordered mesoporous molecular sieves synthesized by a liquid-crystal template mechanism. *Nature*, **359**, 710–712.

Lee, M.Y. and Parkinson, G.M. (1999) Growth rates of gibbsite single crystals determined using in situ optical microscopy. *Journal of Crystal Growth*, **198/199**, 270–274.

Lin, H.P. and Mou, C.Y. (1996) Tubules-within-a-tubule-hierarchical order of mesoporous molecular sieves in MCM-41. *Science*, **273**, 765–768.

Loughnan, F.C. (1969) *Chemical Weathering of the Silicate Minerals*. Elsevier, New York, pp. 27–66.

Lindsay, W.L. and Walthall, P.M. (1996) The solubility of aluminum in soils. Pp. 333–361 in: *The Environmental Chemistry of Aluminum*, 2nd edition (G. Sposito, editor). CRC Lewis, Boca Raton, Florida.

May, H.M., Helmke, P.A., and Jackson, M.L. (1979) Gibbsite solubility and thermodynamic properties of hydroxy-aluminum ions in aqueous solution at 25ºC. *Geochimica et Cosmochimica Acta*, **43**, 861–868.

Monnier, A., Schüth, F., Huo, Q., Kumar, D., Margolese, D., Maxwell, R.S., Stucky, G.D., Krishnamurty, M., Petroff, P., Firouzi, A., Janicke, M. and Chmelka, B.F. (1993) Cooperative formation of inorganic-organic interface in the synthesis of silicate mesostructures. *Science*, **261**, 1299–1303.

Moore, P.B. and Shen, J. (1983) An X-ray structural study of cacoxenite, a mineral phosphate. *Nature*, **306**, 356–358.

Murrell, L.L. (1997) Sols and mixtures of sols as precursors of unique oxides. *Catalysis Today*, **35**, 225–245.

Rathousky, J., Schulzekloff, G., Had, J. and Zukal, A. (1999) Time-resolved in-situ X-ray-diffraction study of mcm-41 structure formation from a homogeneous environment. *Physical Chemistry Chemical Physics*, **1**, 3053–3057.

Schmelzer, J., Pascova, R., Moller, J. and Gutzow, I. (1993) Surface-induced devitrification of glasses: The influence of elastic strain. *Journal of Non-Crystalline Solids*, **162**, 26–39.

Shen, P., Fahn, Y.Y. and Su, A.C. (2001) Imperfect oriented attachment: accretion and defect generation of hexagonal inorganic-surfactant nanoparticles in biomimetic assemblies. *Nano Letters*, **1**, 299–303.

Sinkó, K., Mezei, R., Rohonczy, J. and Fratzl, P. (1999) Gel structures containing Al(III). *Langmuir*, **15**, 6631–6636.

Sweegers, C., Boerrigter, S.X.M., Grimbergen, R.F.P., Meekes, H., Fleming, S., Hiralal, I.D.K. and Rijkeboer, A. (2002) Morphology prediction of gibbsite crystals – An explanation from the lozenge-shaped growth morphology. *The Journal of Physical Chemistry B*, **106**, 1004–1012.

Theng, B.K.G. (1974) *The Chemistry of Clay-organic Reactions*. Wiley, New York, p. 343.

Valeton, I. (1972) *Developments in Soil Science – 1*. Elsevier, Amsterdam, p. 226.

Veesler, S. and Boistelle, R. (1994) Growth kinetics of hydrargillite $Al(OH)_3$ from caustic soda solutions. *Journal of Crystal Growth*, **142**, 177–183.

Violante, A. and Huang, P.M. (1985) Influence of inorganic and organic ligands on the formation of aluminum hydroxides and oxyhydroxides. *Clays and Clay Minerals*, **33**, 181–192.

Wang, W.Z. and Hsu, P.H. (1994) The nature of polynuclear OH-Al complexes in laboratory-hydrolyzed and commercial hydroxyaluminum solutions. *Clays and Clay Minerals*, **42**, 356–368.

Winchell, A.A. and Winchell, H. (1961) Description of minerals. P. 77 in: *Elements of Optical Mineralogy - an Introduction to Microscopic Petrography*, 4th edition, part II. John Wiley & Sons, New York.

Witten, Jr., T.A. and Sander, L.M. (1981) Diffusion-limited aggregation, a kinetic critical phenomenon. *Physical Review Letters*, **47**, 1400–1403.

Yada, M., Machida, M. and Kijima, T. (1996) Synthesis and deorganization of an aluminum-based dodecyl-sulfate mesophase with a hexagonal structure. *Chemical Communications*, **6**, 769–770.

Yada, M., Hiyoshi, H., Ohe, K., Machida, M. and Kijima, T. (1997) Synthesis of aluminum-based surfactant mesophases morphologically controlled through a layer to hexagonal transition. *Inorganic Chemistry*, **36**, 5565–5569.

Yamaguchi, G., Yanagida, H. and Ono, S. (1966) Condition of tohdite $5Al_2O_3.H_2O$ formation. *Journal of Ceramic Association of Japan*, **74**, 84–89.

(*Received 27 January 2003; revised 27 February 2004; Ms. 756; A.E. William F. Jaynes*)